Acta Crystallographica Section D
Biological Crystallography
ISSN 0907-4449

Structural analysis of neprilysin with various specific and potent inhibitors

Christian Oefner,[a] Bernard P. Roques,[b] Marie-Claude Fournie-Zaluski[b] and Glenn E. Dale[a]*

[a]Morphochem AG, CH-4058 Basel, Switzerland, and [b]Department de Pharmacochimie Moleculaire et Structurale, INSERM U266, CNRS UMR 8600, UFR des Sciences Pharmaceutiques et Biologiques, 4 Avenue de l'Observatoire, 75006 Paris, France

Correspondence e-mail: glenn.dale@morphochem.ch

Received 27 October 2003
Accepted 28 November 2003

PDB References: neprilysin–inhibitor complexes, 1r1h, 1r1hsf; 1r1i, r1rlisf; 1r1j, r1rjsf.

Neutral endopeptidase (NEP) is the major enzyme involved in the metabolic inactivation of a number of bioactive peptides including the enkephalins, substance P, endothelin, bradykinin and atrial natriuretic factor. Owing to the physiological importance of NEP in the modulation of nociceptive and pressor responses, there is considerable interest in inhibitors of this enzyme as novel analgesics and antihypertensive agents. Here, the crystal structures of the soluble extracellular domain of human NEP (residues 52–749) complexed with various potent and competitive inhibitors are described. The structures unambiguously reveal the binding mode of the different zinc-chelating groups and the subsite specificity of the enzyme.

1. Introduction

Neprilysin (NEP; EC 3.4.24.11), also known as neutral endopeptidase, enkephalinase, CALLA or CD10, is the prototype of the M13 subfamily of type II integral membrane zinc-dependent endopeptidases. NEP was originally extracted and purified from the brush border of rabbit kidney as a peptidase capable of hydrolyzing the insulin B chain (Kerr & Kenny, 1974). The catalytic properties of NEP resemble those of a group of zinc-dependent bacterial endopeptidases, of which thermolysin (TLN) is the best characterized (Matthews, 1988). NEP is located at the cell surface, with the bulk of the protein, including the active site, facing the extracellular space, and therefore functions as a ectoenzyme catalyzing peptide hydrolysis at the surface of the plasma membrane. It is widely distributed in mammalian tissues and is involved in the inactivation of a variety of signalling peptides (Erdos & Skidgel, 1989; Roques *et al.*, 1993; Turner & Tanzawa, 1997). NEP has been implicated in the regulation of opioid peptide action through the degradation of endogenously released enkephalins (Roques *et al.*, 1980). NEP is involved in the physiological degradation of peptides modulating blood pressure, such as the cardiac hormone atrial natriuretic peptide (ANP), bradykinin and endothelin. More recently, NEP has been implicated in the degradation of amyloid β peptide (Aβ1–42), the primary pathogenic agent in Alzheimer's disease (Shirotani *et al.*, 2001; Iwata *et al.*, 2001). Potent inhibitors of NEP have been synthesized that produce a pharmacological response through increase in opioid or vasoactive peptide levels, indicating their therapeutic potential as novel analgesics or antihypertensive agents (Burnett, 1999; Roques & Beaumont, 1990). However, there is great interest in the identification of novel inhibitors with improved properties for clinical use.

In recent years, several mammalian homologues of NEP have been described, including the endothelin-converting enzymes ECE-1 (Shimada *et al.*, 1994) and ECE-2 (Emoto & Yanagisawa, 1995), the erythrocyte surface antigen KELL (Lee *et al.*, 1991), the phosphate-regulating gene (PEX) on the X chromosome (HYP Consortium, 1995), soluble secreted endopeptidase (SEP; Ikeda *et al.*, 1999) and the recently identified damage-induced neuronal endopeptidase (DINE)/X-converting enzyme (XCE) (Valdenaire *et al.*, 1999; Kiryu-Seo *et al.*, 2000). The overall homology between NEP and the M13 family members ranges from 55 to 25%, but increases if only the 250 C-terminal residues are considered. This degree of similarity is sufficient to indicate that these proteins share a common origin and a similar fold.

The recent elucidation of the structure of the soluble extracellular domain (Asp52–Trp749) of human NEP (sNEP) determined in a complex with phosphoramidon (Oefner *et al.*, 2000) has supported much of the earlier biochemistry and modelling data (Tiraboschi *et al.*, 1999) (Fig. 1). The ectodomain of the protein is composed of two α-helical domains connected by intertwining polypeptide segments. The larger domain includes the residues involved in zinc ligation and catalysis such as the characteristic HE*xx*H zincin motif, which is typical of many zinc peptidases (Hooper, 1994), as well as the conserved consensus sequence E*xx*A/GD in which the glutamate serves as the third zinc ligand

(Roques *et al.*, 1993). This domain shows similarity with thermolysin and other related microbial metalloproteases.

In order to identify the interactions stabilizing inhibitor binding and further understand the mode of enzyme inhibition, with the aim of designing new NEP inhibitors that are active *in vivo*, complexes with various potent and selective inhibitors have been solved by X-ray crystallography. The soluble extracellular domain of human NEP was expressed in yeast and the protein purified to homogeneity as described by Dale *et al.* (2000). Crystals could be obtained of the Endo-F1 glycosidase-treated enzyme in the presence of the inhibitors. The binary complexes were solved using the protein coordinates of sNEP present in a complex with phosphoramidon (PDB code 1dmt) as the starting model.

Table 1
Data-collection and refinement statistics.

	sNEP–(1)	sNEP–(2)	sNEP–(3)
Unit-cell parameters (Å)	a = 107.8, c = 113.1	a = 108.8, c = 113.1	a = 107.5, c = 112.0
Resolution range (outer shell) (Å)	20.0–1.95 (2.07–1.95)	20.0–2.55 (2.75–2.55)	20.0–2.35 (2.50–2.35)
No. observed reflections	384.416	107.787	130.858
No. unique reflections	53.437	25.414	31.584
R_{sym}† (overall/outer shell) (%)	6.2/46.3	6.6/27.2	9.0/48.0
$I/\sigma(I)$ (overall/outer shell)	26.2/2.5	15.9 /2.5	14.7/3.1
Completeness (overall/outer shell) (%)	95.9/93.4	99.2/100	99.8/99.9
Refinement statistics			
Resolution range (Å)	20–1.95	20–2.60	20–2.35
R_{cryst}‡ (%)	20.9	28.0	22.2
R_{free}‡ (%)	26.0	35.8	28.3
No. protein atoms (mean B, Å^2)	5595 (28.2)	5595 (53.8)	5595 (31.9)
No. water molecules	295	19	88
No. ligand atoms (mean B, Å^2)	29 (20.0)	26 (47.8)	28 (39.2)
No. NAG atoms (mean B, Å^2)	42 (43.7)	42 (69.4)	42 (50.3)
R.m.s.d.§ bonds (Å^2)	0.007	0.013	0.005
R.m.s.d.§ angles (°)	0.86	1.49	0.72

† $R_{sym} = \sum_h \sum_i |I_i(h) - \langle I \rangle| / \sum_h \sum_i I(h)$, where $I_i(h)$ and $\langle I(h) \rangle$ are the ith and mean measurement of the intensity of reflection h. ‡ $R_{cryst} = \sum_h ||F_{obs}| - |F_{calc}|| / \sum_h |F_{obs}|$, where $|F_{obs}|$ and $|F_{calc}|$ are the observed and calculated structure-factor amplitudes for the reflection h, applied to the working set. R_{free} is the same but applied to the test set. § R.m.s.d.: root-mean-square deviation from mean.

2. Materials and methods

2.1. Crystallization, data collection and refinement

Protein in 25 m*M* Tris pH 7.0, 150 m*M* NaCl and 2 m*M* $MgCl_2$ was concentrated to 20 mg ml^{-1} and treated with glycosidase Endo-F to remove N-linked sugars as described by Gruenunger-Leitch *et al.*, 1996). Binary complexes of the glycosidase-treated sNEP were formed with the three inhibitors at a concentration of 1 m*M*. Crystals of the inhibited protein were obtained by vapour diffusion with 25% PEG 3350, 200 m*M* ammonium sulfate, 100 m*M* bis-tris pH 7.5 as the precipitating agent (Dale *et al.*, 2000). They belong to the trigonal space group $P3_221$, with one molecule in the asymmetric unit. All crystals were flash-frozen in a cryoprotectant solution corresponding to the reservoir conditions containing 30% glycerol and data were collected at 100 K. All data sets, except that for the binary complex with (2), were measured with Cu $K\alpha$ radiation provided by a Nonius FR591 rotating-anode generator equipped with an Osmic mirror system. Diffraction intensities were recorded on a MAR Research image-plate area detector. The data set for (2) was collected at SLS beamline X06SA at PSI, Villigen, Switzerland on a MAR CCD detector at a wavelength of 0.9 Å. All diffraction data were processed and scaled with *DENZO* and *SCALEPACK* (Otwinowski, 1993) and further analyzed with the *CCP*4 program suite (Collaborative Computational Project, Number 4, 1994). The refinement protocols for all data sets followed the same procedure using the refined protein coordinates of human sNEP present in a complex with phosphoramidon (PDB code 1dmt; Oefner *et al.*, 2000). At the beginning of the refinement, the phosphoramidon inhibitor and all solvent molecules were removed from the model. Iterative rounds of model building were performed with *MOLOC* (Gerber, 1992) and stereochemically restrained positional and temperature-factor refinement was performed with *REFMAC* (Murshudov *et al.*, 1997), using parameters for ideal stereochemistry as described by Engh & Huber (1991). In each complex structure, a difference Fourier map revealed a residual electron density located in the active site corresponding to the bound small molecule. Progressive introduction of solvent molecules with good geometry lead to binary complexes lacking the two N-terminal residues Asp52 and Asp53. Only the crystals for compound (2) showed anisotropic X-ray diffraction, leading to anisotropic thermal ellipsoids of 2.1, 2.1 and −3.2 Å^2 along the crystal axes and resulting in a relatively high R_{work} and R_{free}. All final electron densities are of high quality and the inhibitors are well defined (Fig. 2). Data-collection and refinement statistics are summarized in Table 1.

3. Results and discussion

All inhibitors are nestled in the interior of the enzyme cavity and bind, similar to phosphoramidon, near the highly conserved residues of the consensus sequences ^{583}HE*xx*H^{587} and ^{646}E*xxx*D^{650} and the residues of the ^{542}NAFY^{545} motif. In every complex structure the amino-acid side chains of His583, His587 and Glu646 are involved in zinc ligation, together with a monodentate or bidentate recognition depending on the ligand. Fig. 2 shows the final $2F_o - F_c$ electron densities for all inhibitors calculated with phases from the refined models together with their electrophilic interactions with the enzyme. In the complex with (1) the zinc ion is coordinated in an approximately tetrahedral geometry. Its monodentate recognition by the inhibitor involves a single O atom of a tetrahedral phosphinic group with an interatomic distance of 1.94 Å, in addition to the three ligands from the protein, His583 (2.04 Å), His587 (2.12 Å) and Glu646 (1.98 Å). The crystal structure reveals that Glu584 forms a strong hydrogen bond to the second O atom of the phosphinic moiety with an interatomic distance of 2.42 Å, replacing the catalytic water molecule, which is polarized by the acidic side chain during catalysis (Devault *et al.*, 1988). Within this and all the other ligand-binding complexes, the zinc ion is inaccessible to solvent and close to the inner surface of the protein, which is structurally most closely related to other zinc metalloproteases such as thermolysin (Matthews, 1988), bacterial metallo-elastase (Thayer *et al.*, 1991) and the neutral protease from *Bacillus cereus* (Pauptit *et al.*, 1988).

The free terminal amino group of the inhibitor stabilizes the complex by forming a hydrogen bond with the main-chain carbonyl O atom of Ala543 (2.73 Å). The free amino group has been introduced in (1) in order to obtain a dual NEP/APN inhibitor (Chen *et al.*, 2000). This function is not essential for NEP recognition, but it is interesting to observe that this group is involved in the stabilization of the inhibitor by interaction with the carbonyl of Ala543.

This residue, found in the ^{542}NAFY^{545} consensus motif of the M13 metallopeptidase family, is generally involved in a hydrogen bond with the NH of the P_1' residue. This is illustrated for compounds (2) and (3). The presence in (1) of a CH_2 in place of an NH displaces the hydrogen bonding towards the free amino groups. However, the methyl moiety of the P_1 residue of the inhibitor is exposed to solvent and plays a similar role in ligand binding as the rhamnose moiety of phosphoramidon. It is not in direct contact with the protein, reflecting the minor stabilizing role of the S_1 subsite in NEP (Ksander *et al.*, 1997). The side chain of Arg717, which participates in a salt bridge with Asp650, interacts with the inhibitor by forming two hydrogen bonds with the carbonyl O atom of the biphenyl moiety in the P_1' position. Further hydrophilic interactions are provided by the side chain of Asn542. It functions as a hydrogen-bond acceptor and donor group and interacts with the amino and C-terminal carboxyl groups of the P_2' residue of the inhibitor, with hydrogen-bonding distances of 2.97 and 3.04 Å, respectively. The large hydrophobic biphenyl moiety of the inhibitor is positioned in the S_1' subsite of sNEP (Fig. 3). This is in agreement with the subsite specificity for large hydrophobic P_1' residues (Tiraboschi *et al.*, 1999). The deep lipophilic cavity of the subsite has a volume of approximately 420 Å^3. It is formed by the side chains of Phe106, Ile558, Phe563, Met579, Val580, Val692 and Trp693 and is nicely filled with the side chain of the hydrophobic P_1' residue, with both phenyl moieties being tilted by approximately −45°. The side chains of Met579 and Trp693 point towards the face of the second phenyl from opposite sites.

The refined structures of the binary complexes of sNEP with (2) and (3) clearly show that both compounds interact through bidentation with the Zn atom. Both the S and the O atom of the mercaptoacyl function bind to the metal with interatomic distances of 2.4 and 1.8 Å as well as 2.1 and 1.8 Å, respectively. In both complexes the five zinc ligands form a distorted trigonal bipyramid. His587 NE2 and the carbonyl O atom of the inhibitor occupy axial positions, while the sulfur ligand SG and the coordinating enzyme amino acids His583 NE2 and Glu646 OE1 are in planar positions. In such a conformation the main-chain carbonyl O atom of the conserved P_1 residue is close to NE2 of the side chain of His583 and adopts a

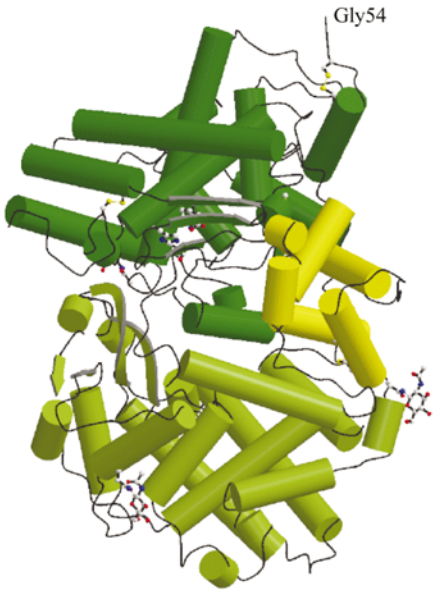

Figure 1
Cartoon model of human neprilysin, showing the larger catalytic domain in forest green, the smaller domain in light green and the three inter-domain linker fragments in yellow. The catalytic site is located on the inner surface of the structure and bears the conserved amino acids involved in zinc ligation and catalysis.

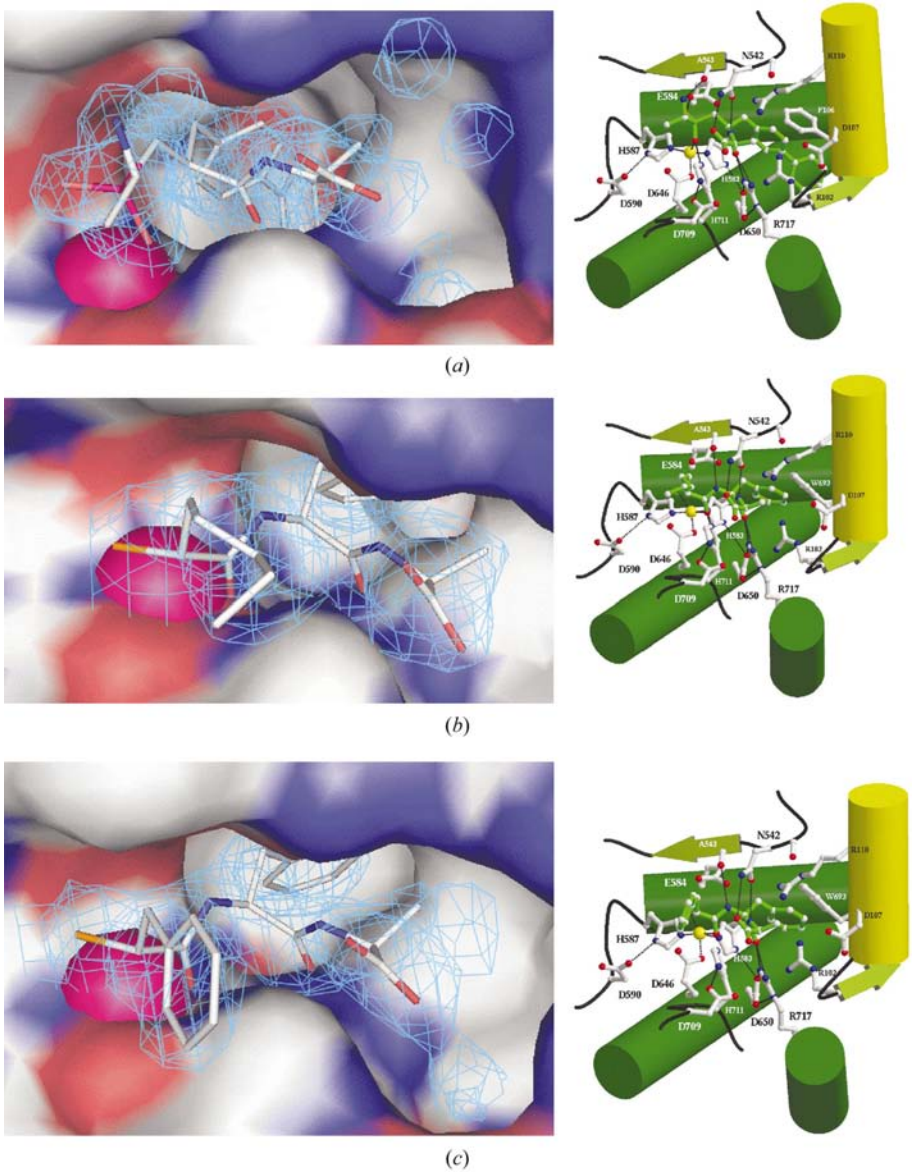

Figure 2
$2F_o - F_c$ electron-density maps for compounds (1) (*a*), (2) (*b*) and (3) (*c*) calculated with phases from the superimposed refined model. All maps are contoured at 1σ and are shown in cyan mesh. The molecular surface of the S_1' subsite is indicated and coloured by electrostatic potential: blue, positive; red, negative. The Zn atom is shown as a pink sphere. The figures were generated using *PyMOL* (DeLano, 2001). The right-hand panels show the electrophilic interactions of the inhibitors with the enzyme. Helices are shown as tubes and sheets are shown as arrows. Hydrogen bonds are indicated by dashed lines. These figures were generated with the prograns *MOLSCRIPT* (Kraulis, 1991) and *Raster3D* (Merritt & Bacon, 1997).

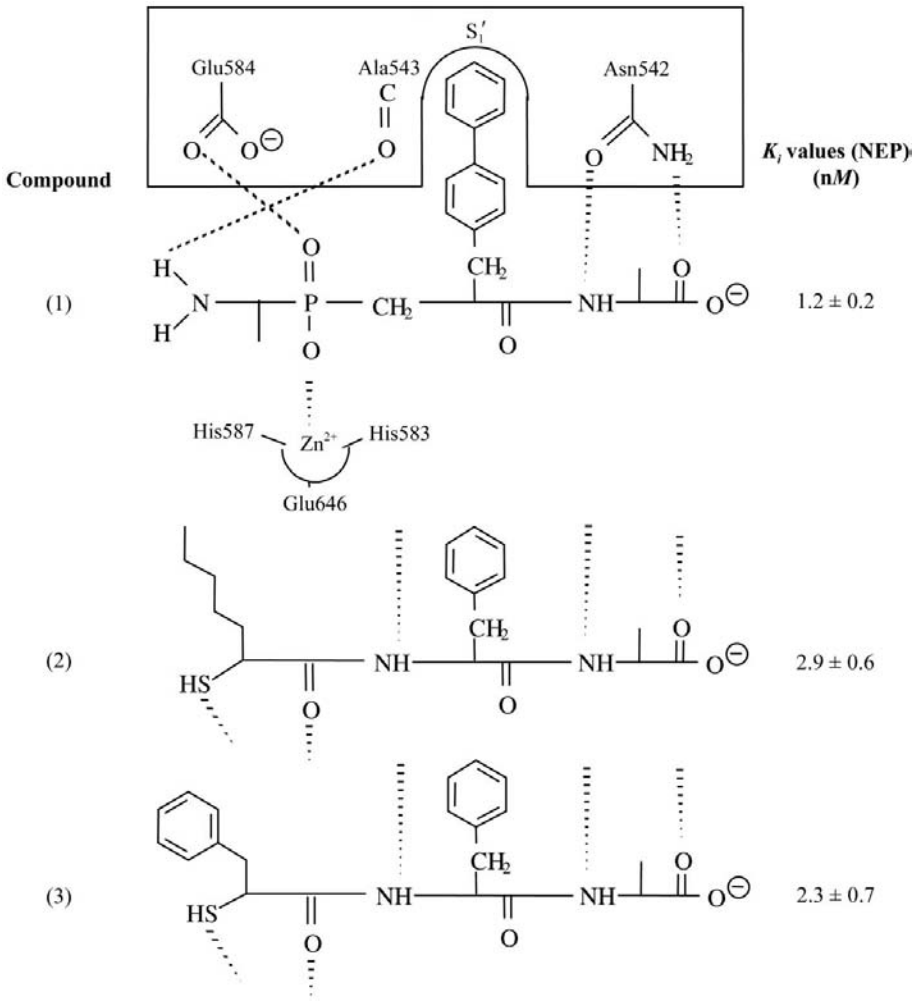

Figure 3
Binding modes of compounds (1), (2) and (3) to the active site of human sNEP. Intermolecular hydrogen bonds are indicated by dashed lines.

position similar to that of the O atom of the cleavable peptide bond of the substrate. The SH group of both compounds occupies a similar position and points towards the side chain of Glu584, while replacing the catalytic water molecule. Taking into account the large preference of the NEP S_1' subsite for aromatic residues, the structure obtained for the NEP–(2) complex was expected. However, this result was not as obvious for the complex with (3). Indeed, this compound has two benzylic moieties which in principle could fit the S_1'/S_2' domain of the enzyme, pushing the C-terminal alanine residue outside the active-site cleft. Such a recognition mode is associated with zinc monodentation. The crystallographic data demonstrate that this hypothesis in incorrect, very likely because zinc bidentation increases the complex stability. Compounds (2) and (3) do not differ in their C-terminal extension and again show the same intermolecular interactions with the enzyme, reflecting the minor stabilizing role of the S_1 subsite. In both complexes, the S_1' subsite binds the central hydrophobic benzyl moiety of both inhibitors, leaving a cavity with a volume of approximately 190 Å^3 unoccupied. The differences in the recognition of the biphenyl moiety of compound (1) and the benzyl moiety of compounds (2) and (3) is a side-chain alteration of residues Met579 and Trp693 within the subsite. The position of their P_2' residue and the interactions of their backbone with the enzyme, however, are comparable to that of compound (1).

For all three compounds, the carboxy-terminal L-alanine residue is similarly recognized by residues of the S_2' subsite, which extends into the solvent towards the side chains of Arg102, Asp107 and Arg110. In all cases the methyl moiety is within van der Waals contact distance of the side chain of Phe106, which slightly alters its conformation depending on the size of the P_1' residue. The S_2' subsite of sNEP shows reduced specificity and can accommodate more bulky side chains. It is worth mentioning that none of the charged residues of this binding site are directly involved in inhibitor binding.

Depending on the size of the P_1' substituent, the volume of the subsite is altered mainly owing to the indole movement of Trp693. With a bulky substituent, the side chain moves towards the 2′ subsite. This alters the side-chain orientation of Phe106, resulting in a reduced volume of this recognition pocket. This is clearly illustrated by measuring the inhibitory potencies for NEP of various analogues of (1) differing only in their C-terminal residues (Chen *et al.*, 2000). Thus, the K_i values are modulated by the size of the P_2' residue: a K_i value of 0.9 nM is obtained with a glycine residue, 2 nM with an alanine, 11.8 nM with a serine and 32.5 nM with a threonine. Smaller P_1' substituents therefore allow the presence of both either small or large P_2' residues. The simultaneous presence of two large substituents would require a major induced fit involving the linker helix A3, which contains Phe106.

4. Conclusions

The information provided by the three-dimensional structures of the various binary complexes leads to an understanding of the interactions stabilizing inhibitor binding. It gives insight into the zinc ligation and subsite specificity of the enzyme and presents an attractive challenge to increase the potency and selectivity of known inhibitor classes through docking studies in order to support the design of potential modulators of NEP *in vivo*.

We gratefully acknowledge the assistance of A. D'Arcy in crystallization and thank Dr Clemens Schulze-Briese at the SLS protein crystallography beamline X06SA, Paul Scherrer Institute, Villigen, Switzerland, for his experimental help and advice.

References

Burnett, J. C. (1999). *J. Hypertens. Suppl.* **17**, s37–s43.
Chen, H., Noble, F., Mothé, A., Meudal, H., Coric, P., Danascimento, S., Roques, B. P., George, P. & Fournié-Zaluski, M. C. (2000). *J. Med. Chem.* **43**, 1398–1408.
Collaborative Computational Project, Number 4 (1994). *Acta Cryst.* D**50**, 760–763.
Dale, G. E., D'Arcy, B., Yuvaniyama, C., Wipf, B., Oefner, C. & D'Arcy, A. (2000). *Acta Cryst.* D**56**, 894–897.

DeLano, W. L. (2001). *The PyMOL User's Manual.* San Carlos, CA, USA: DeLano Scientific.
Devault, A., Sales, N., Nault, C., Beaumont, A., Roques, B. P., Crine, P. & Boileau, G. (1988). *FEBS Lett.* **231**, 54–58.
Emoto, N. & Yanagisawa, M. (1995). *J. Biol. Chem.* **270**, 15262–15268.
Engh, R. & Huber, R. (1991). *Acta Cryst.* A**47**, 392–400.
Erdos, E. G. & Skidgel, R. A. (1989). *FASEB J.* **3**, 145–151.
Gerber, P. (1992). *Biopolymers*, **32**, 1003–1017.
Gruenunger-Leitch, F., D'Arcy, A., D'Arcy, B. & Chene, C. (1996). *Protein Sci.* **12**, 2617–2622.
Hooper, N. M. (1994). *FEBS Lett.* **354**, 1–6.
HYP Consortium (1995). *Nature Genet.* **11**, 130–136.
Ikeda, K., Emoto, N., Raharjo, S. B., Nurhantari, Y., Saiki, K., Yokoyama, M. & Matsuo, M. (1999). *J. Biol. Chem.* **274**, 32469–32477.
Iwata, N., Tsubuki, S., Takaki, Y., Shirotani, K., Lu, B., Gerard, N. P., Gerard, C., Hama, E., Lee, H. J. & Saido, T. C. (2001). *Science*, **292**, 1550–1552.
Kerr, M. A. & Kenny, A. J. (1974). *Biochem. J.* **137**, 477–488.
Kiryu-Seo, S., Sasaki, M., Yokohama, H., Nakagomi, S., Hirayama, T., Aoki, S., Wada, K. & Kiyama, H. (2000). *Proc. Natl Acad. Sci. USA*, **97**, 4345–4350.
Ksander, G. M., de Jesus, R., Yuan, A., Ghai, R. D., Trapani, A., McMartin, C. & Bohacek, R. (1997). *J. Med. Chem.* **40**, 495–505.
Kraulis, P. J. (1991). *J. Appl. Cryst.* **24**, 946–950.
Lee, S., Zambas, E. D., Marsh, W. L. & Redman, C. M. (1991). *Proc. Natl Acad. Sci. USA*, **88**, 6353–6357.
Matthews, B. W. (1988). *Acc. Chem. Res.* **21**, 333–340.
Merritt, E. A. & Bacon, D. J. (1997). *Methods Enzymol.* **277**, 505–524.
Murshudov, G. N., Vagin, A. A. & Dodson, E. J. (1997). *Acta Cryst.* D**53**, 240–255.
Oefner, C., D'Arcy, A., Hennig, M., Winkler, F. K. & Dale, G. E. (2000). *J. Mol. Biol.* **296**, 341–349.
Otwinowski, Z. (1993). *Proceedings of the CCP4 Study Weekend. Data Collection and Processing*, edited by L. Sawyer, N. Isaacs & S. Bailey, pp. 56–62. Warrington: Daresbury Laboratory.
Pauptit, R. A., Karlsson, R., Picot, D., Jenkins, J. A., Niklaus-Reimer, A. S. & Jansonius, J. N. (1988). *J. Mol. Biol.* **199**, 525–537.
Roques, B. P. & Beaumont, A. (1990). *Trends Pharmacol. Sci.* **11**, 245–249.
Roques, B. P., Fournié-Zaluski, M. C., Soroca, E., Lecomte, J. M., Malfroy, B., Llorens, C. & Schwartz, J. C. (1980). *Nature (London)*, **288**, 286–288.
Roques, R. P., Noble, F., Dauge, V., Fournie-Zaluski, M.-C. & Beaumont, A. (1993). *Pharmacol. Rev.* **45**, 87–146.
Shimada, K., Takahashi, M. & Tanzawa, K. (1994). *J. Biol. Chem.* **269**, 18275–18278.
Shirotani, K., Tsubuki, S., Iwata, N., Takaki, Y., Harigaya, W., Maruyama, K., Kiryu-Seo, S., Kiyama, H., Iwata, H., Tomita, T., Iwatsubo, T. & Saido, T. C. (2001). *J. Biol. Chem.* **276**, 21895–21901.
Thayer, M. M., Flaherty, K. M. & McKay, D. B. (1991). *J. Biol. Chem.* **266**, 2864–2871.
Tiraboschi, G., Jullian, N., Thery, V., Antonczak, S., Fournie-Zaluski, M.-C. & Roques, B. P. (1999). *Protein Eng.* **12**, 141–149.
Turner, A. J. & Tanzawa, K. (1997). *FASEB J.* **11**, 355–364.
Valdenaire, O., Richards, J. G., Faull, R. L. & Schweizer, A. (1999). *Brain Res. Mol. Brain Res.* **64**, 211–221.